

Fast computation of temperature and polarization coupling matrices

Georgia Kiddier,¹★ and Steven Gratton^{1,2}†

¹Centre for Theoretical Cosmology, Department of Applied Mathematics and Theoretical Physics,

University of Cambridge, Wilberforce Road, Cambridge, CB3 0WA, UK

²Kavli Institute for Cosmology Cambridge, Madingley Road, Cambridge, CB3 0HA, UK

17 February 2026

ABSTRACT

We present a fast and exact method for computing CMB mode-coupling matrices based on an optimised evaluation of Wigner-3 j symbols. The method exploits analytic structure in the relevant Wigner-3 j symbol configurations appearing in temperature and polarization coupling matrices, expressing all required quantities in terms of a small set of recurrence-generated values which are precomputed and stored in lookup tables. This approach reduces the computational cost of constructing the full coupling matrices whilst maintaining numerical accuracy.

We demonstrate the performance of the `threej_cosmo` implementation using realistic survey masks from current CMB experiments. Relative to standard recursion-based approaches used in existing pseudo- C_ℓ pipelines, the method achieves speedups of 6–25× in practical coupling-matrix constructions, with the largest gains occurring at high multipoles. The algorithm admits efficient parallelisation on both CPUs and GPUs, the latter providing additional acceleration, up to a further $\mathcal{O}(50)$ on modern hardware, without altering the underlying formalism.

Beyond full matrix construction, the approach is naturally suited to applications in which only a restricted set of ℓ_3 modes is required for each (ℓ_1, ℓ_2) pair, such as in the computation of band-limited coupling matrices and analytic covariance terms. These features make `threej_cosmo` a practical backend for pseudo- C_ℓ estimation and related calculations in next-generation CMB analysis pipelines.

Key words: methods: numerical – methods: data analysis – cosmic background radiation

1 INTRODUCTION

The cosmic microwave background (CMB), first discovered in 1965 (Penzias & Wilson 1965) and whose fluctuations were detected by the COBE satellite in 1992 (Smoot et al. 1992), has become one of the most powerful probes of cosmological parameters. WMAP (Hinshaw et al. 2013) and the Planck mission (Planck Collaboration 2020) subsequently measured the CMB temperature and polarization anisotropies with unprecedented precision, constraining the standard Λ CDM model to percent-level accuracy. Much of the constraining power for cosmology from CMB anisotropies comes from their angular power spectra generically denoted C_ℓ , with ℓ being angular multipole number. Forthcoming CMB experiments such as the Simons Observatory (Simons Observatory Collaboration 2019) will provide an order of magnitude more data, reaching arcminute resolution across large sky areas.

Observations of the CMB are contaminated by foreground emissions such as Galactic synchrotron, thermal dust, and unresolved point sources. To suppress these contaminants, standard analyses apply sky masks that disregard polluted regions of the sky. Such masking also induces mode coupling in spherical harmonic space.

The pseudo- C_ℓ method provides an efficient way to perform an analysis on the masked sky, relating the expectation of the observed

pseudo-spectrum to the underlying power spectrum through a linear relationship that accounts for the masking of the sky (Wandelt et al. 2001; Hivon et al. 2002; Efstathiou 2004; Alonso et al. 2019). This is done through the introduction of the mode-coupling matrix $K_{\ell_1 \ell_2}$, which can in turn be expressed in terms of the window function W_ℓ , the harmonic power spectrum of the mask. Unlike maximum likelihood estimators, which scale with multipole as $\mathcal{O}(\ell_{\max}^6)$, the pseudo- C_ℓ method achieves a more tractable computational scaling of $\mathcal{O}(\ell_{\max}^3)$. This makes it well suited for high-resolution surveys such as Planck, ACT (Naess et al. 2025), and the Simons Observatory.

The MASTER algorithm (Hivon et al. 2002) is a widely used implementation of this formalism and forms the basis for several public pipelines, including `pspy`¹. Efficient and accurate evaluation of the coupling matrix $K_{\ell_1 \ell_2}$ is therefore important to the performance of pseudo- C_ℓ -based estimators and is a key focus of this work. A significant amount of time is spent in the recursion formulae used to calculate Wigner-3 j symbols, see e.g. Edmonds (1957), hereafter E57, that are contained within the elements of $K_{\ell_1 \ell_2}$. At the heart of this computation is the algorithm of Schulten & Gordon (1975), which uses recurrence relations for exact evaluation of the 3 j symbols of the form

$$\left(\begin{array}{ccc} \ell_1 & \ell_2 & \ell_3 \\ m_1 & m_2 & m_3 \end{array} \right). \quad (1)$$

★ E-mail: glk27@cam.ac.uk

† E-mail: stg20@cam.ac.uk

¹ <https://github.com/simonsobs/pspy>

This is implemented in the publicly available SLATEC Fortran library, more specifically in the subroutine DRC3jj². For fixed ℓ_2 and ℓ_3 this routine evaluates the $3j$ symbol for all allowed values of ℓ_1 , with all other parameters fixed, satisfying $m_1 + m_2 + m_3 = 0$ and obeying the triangular inequality $|\ell_2 - \ell_3| \leq \ell_1 \leq \ell_2 + \ell_3$. The subroutine is used for mode-coupling matrix calculation in current CMB pipelines, with $m_1 = m_2 = m_3 = 0$ for temperature and also $m_1 = -2, m_2 = 2, m_3 = 0$ when including polarization. Pseudo- C_ℓ mode-coupling matrices of the same form as those used in CMB analyses also arise in projected LSS angular power spectra (Lizancos & White 2024).

Wigner- $3j$ symbols also appear in the covariance of pseudo- C_ℓ estimates. While the exact expression is computationally expensive, involving sums over magnetic indices, useful approximations exist (Efstathiou 2004; Brown et al. 2005). Here the computation is reduced to one essentially equivalent to computing a mode coupling matrix.

Some recent work has been done to speed up the computation of mode-coupling matrices, such as using the Toeplitz approximation for diagonal-constant matrices (Louis et al. 2020). This approximation is shown to be highly accurate in power spectrum estimation, but is not exact for all multipoles in the coupling matrix because the structure is not exactly Toeplitz for all values of ℓ .

Beyond pseudo- C_ℓ estimation, Wigner- $3j$ symbols also appear in several other areas of CMB and large-scale structure analysis. Lensing of the CMB induces off-diagonal covariance between multipoles proportional to the lensing potential.

Wigner symbols with magnetic numbers $(0, -1, 1)$ then appear in the weight function of the optimal quadratic estimator for the lensing potential (see Okamoto & Hu (2003) and e.g. Planck Collaboration (2014a)). The same symbol also appears in the analysis of the aberration of the CMB (see e.g. Planck Collaboration (2014b)).

Related structures also appear in higher-order analyses. In recent work on fast skew-spectrum and projected bispectrum estimators, the leading covariance contribution is shown to have a summation structure closely analogous to the pseudo- C_ℓ mode-coupling matrix (Harscoubet et al. 2025).

These examples highlight that accelerating Wigner-symbol evaluation is beneficial not only for pseudo- C_ℓ power-spectrum estimation, but also more widely in cosmological analyses. This paper outlines a method for simplified evaluation of such $3j$ symbols. An associated code, `threej_cosmo`, implements this approach³ and may be integrated into pseudo- C_ℓ estimation pipelines.

The paper is organized as follows. Section 2 outlines the pseudo- C_ℓ estimation method and motivates the optimisation of the coupling matrix calculations. Section 3 derives the recursion relations that form the basis for the fast evaluation of $3j$ symbols. Section 4 benchmarks the algorithm using ACT DR6 survey window functions (Naess et al. 2025) and compares performance with existing routines. We conclude in Sec. 5, and two appendices provide further mathematical details.

2 PSEUDO- C_ℓ ESTIMATION

In this section we outline the standard pseudo- C_ℓ algorithm for estimating an unbiased power spectrum using mode-coupling matrices $K_{j_1 j_2}$ (see e.g. Hivon et al. (2002); Efstathiou (2004)). For notational consistency with the angular-momentum literature, we write

² Available from <http://www.netlib.org/slatec/src/drc3jj.f>

³ https://github.com/gkiddier22/threej_cosmo

j in place of ℓ . Since our focus is on accelerating the evaluation of Wigner- $3j$ symbols, here we restrict attention to the TT and EE coupling matrices, which already contain the two symbol configurations that appear in the full set of pseudo- C_ℓ estimators; fuller details are provided in Appendix A.

At a given frequency, the expectation values of the pseudo-spectra satisfy

$$\begin{aligned} \langle \tilde{C} \rangle^{T_i T_j} &= K^{T_i T_j} C^{TT}, \\ \langle \tilde{C} \rangle^{E_i E_j} &= K^{E_i E_j} C^{EE} + K^{E_i B_j} C^{BB}, \end{aligned} \quad (2)$$

where $\tilde{C}^{X_i X_j}$ denotes the cross spectrum between two masked CMB maps X_i and X_j , and C^{TT} , C^{EE} and C^{BB} denote the underlying temperature-, E-mode-, and B-mode-power spectra, respectively. The mode-coupling matrices take the form

$$\begin{aligned} K_{j_1 j_2}^{T_i T_j} &= \frac{(2j_2 + 1)}{4\pi} \sum_{j_3} (2j_3 + 1) \tilde{W}_{j_3}^{T_i T_j} \begin{pmatrix} j_1 & j_2 & j_3 \\ 0 & 0 & 0 \end{pmatrix}^2 \\ &\equiv (2j_2 + 1) \Xi_{TT}(j_1, j_2, \tilde{W}^{T_i T_j}), \end{aligned} \quad (3)$$

$$\begin{aligned} K_{j_1 j_2}^{E_i P_j} &= \frac{(2j_2 + 1)}{4\pi} \sum_{j_3} (2j_3 + 1) \tilde{W}_{j_3}^{P_i P_j} \left(\frac{1 \pm (-1)^J}{2} \right)^2 \\ &\quad \times \begin{pmatrix} j_1 & j_2 & j_3 \\ -2 & 2 & 0 \end{pmatrix}^2 \\ &\equiv (2j_2 + 1) \Xi_{EP}(j_1, j_2, \tilde{W}^{P_i P_j}), \end{aligned} \quad (4)$$

where $P_j \in \{E, B\}$ and $J \equiv j_1 + j_2 + j_3$. Here $\tilde{W}_\ell^{X_i Y_j}$ is the harmonic power spectrum of the survey window function, obtained from the auto- or cross-spectrum of the masks applied to the maps X_i and Y_j .

The parity structure of these expressions is worth emphasising, in particular their dependence on whether J is even or odd. The temperature symbol

$$\begin{pmatrix} j_1 & j_2 & j_3 \\ 0 & 0 & 0 \end{pmatrix},$$

which we may generically denote by $\mathcal{J}_{(0,0)}$, vanishes for odd J , so TT receives contributions only from even-parity configurations. In contrast, the polarization symbol

$$\begin{pmatrix} j_1 & j_2 & j_3 \\ -2 & 2 & 0 \end{pmatrix},$$

which we may generically denote by $\mathcal{J}_{(-2,2)}$, is non-zero for both even and odd J . The relevant parity projection is instead enforced by the factors $(1 \pm (-1)^J)^2$ in Eq. (4): the + sign selects even J (as in the EE matrix), while the - sign selects odd J (as in the EB matrix). Consequently, although the $\mathcal{J}_{(-2,2)}$ symbol itself is non-zero for both parities, only its even- J component enters K^{EE} , while only the odd- J component enters K^{EB} . These selection rules will be useful when deriving the optimized recurrence relations in Section 3, where we explicitly separate the even- and odd- J branches of the $\mathcal{J}_{(-2,2)}$ symbols and show how both can be expressed in terms of the $\mathcal{J}_{(0,0)}$ symbols.

In summary, to compute all elements of the coupling matrices, we require Wigner- $3j$ symbols of the form

$$\begin{pmatrix} j_1 & j_2 & j_3 \\ 0 & 0 & 0 \end{pmatrix}, \quad (5)$$

and

$$\begin{pmatrix} j_1 & j_2 & j_3 \\ -2 & 2 & 0 \end{pmatrix}. \quad (6)$$

In this work we use the calculation of the $K^{T_i T_j}$ and $K^{E_i E_j}$ mode-coupling matrices as representative benchmarks for the efficiency of our Wigner- $3j$ computations, noting that the same symbols also enter analytic pseudo- C_ℓ covariance calculations (Efstathiou 2004; Brown et al. 2005).

As shown in Efstathiou (2004), the exact evaluation of the covariance expression is computationally impractical at high multipoles, and one instead considers an approximation motivated by a simplification that occurs when the CMB power spectrum does not vary over the band limit of the mask. In this limit, the pseudo- C_ℓ covariance reduces to a kernel constructed from the power spectrum of the squared mask.

Consequently, approximate covariance constructions in this regime involve exactly the same classes of Wigner- $3j$ symbols as those appearing in the coupling matrices, including both $(m_1, m_2, m_3) = (0, 0, 0)$ and, for polarization, $(m_1, m_2, m_3) = (-2, 2, 0)$ configurations. The fast evaluation techniques developed in this work therefore apply directly to the efficient computation of such approximate pseudo- C_ℓ covariance terms.

We first simplify the computation of the $3j$ symbols with all m indices equal to zero, i.e. the $\mathcal{J}_{(0,0)}$ above. We then use recursion relations to express the symbols with $(m_1, m_2, m_3) = (-2, 2, 0)$, i.e. the $\mathcal{J}_{(-2,2)}$. In deriving the latter, we also derive expressions for $3j$ symbols with $(m_1, m_2, m_3) = (-1, 1, 0)$, which we may denote $\mathcal{J}_{(-1,1)}$.

For the polarization coupling matrices that involve $3j$ symbols as in Eq. (6), our implementation first computes the equivalent $(0, -2, 2)$ configuration using the optimized recursion relations derived in Section 3, and then applies the permutation symmetry of the $3j$ symbols,

$$\begin{pmatrix} j_1 & j_2 & j_3 \\ m_1 & m_2 & m_3 \end{pmatrix} = \begin{pmatrix} j_2 & j_3 & j_1 \\ m_2 & m_3 & m_1 \end{pmatrix}, \quad (7)$$

to obtain the required $(-2, 2, 0)$ configuration.

3 FAST COMPUTATION ALGORITHM

The mode-coupling matrices considered in this work depend on Wigner- $3j$ symbols of the form

$$\begin{pmatrix} j_1 & j_2 & j_3 \\ 0 & 0 & 0 \end{pmatrix}, \quad \begin{pmatrix} j_1 & j_2 & j_3 \\ -2 & 2 & 0 \end{pmatrix},$$

which enter squared in the TT and EE coupling matrices (see Eqs. 3 and 4), and appear as products of the two symbols in the TE case (see Eq. A2).

For fixed (j_1, j_2) the coupling kernels require summation over j_3 in steps of two, reflecting the constraint that $J = j_1 + j_2 + j_3$ must be even, for TT, TE, EE and BB, or odd, for EB. The combinations

$$\begin{aligned} J &= j_1 + j_2 + j_3, \\ J_{-++} &= -j_1 + j_2 + j_3, \\ J_{+-+} &= j_1 - j_2 + j_3, \\ J_{++-} &= j_1 + j_2 - j_3. \end{aligned} \quad (8)$$

therefore change by ± 2 when $j_3 \mapsto j_3 + 2$. Since the allowed values of j_3 enforce integer parity of these combinations, it is convenient to introduce the halved variables

$$p = J/2, \quad p_1 = J_{-++}/2, \quad p_2 = J_{+-+}/2, \quad p_3 = J_{++-}/2,$$

which change by ± 1 between successive terms in the sum. In coupling matrix calculations this structure allows the summation over j_3 to be

implemented as a simple recurrence, with each new term obtained from the previous one using integer-index updates and a small number of floating-point operations.

3.1 Squared Symbol $\mathcal{J}_{(0,0)}$

Equations (3.7.4) and (3.7.5) of E57 state that a $3j$ symbol remains unchanged under even permutations of its columns while an odd permutation introduces a factor of $(-1)^J$. Additionally, from E57 Eq. (3.7.6), flipping the signs of all m -values also results in a factor of $(-1)^J$:

$$\begin{pmatrix} j_1 & j_2 & j_3 \\ -m_1 & -m_2 & -m_3 \end{pmatrix} = (-1)^J \begin{pmatrix} j_1 & j_2 & j_3 \\ m_1 & m_2 & m_3 \end{pmatrix}. \quad (9)$$

Thus for example such a symbol with $m_i = 0$ may be non-zero only if J is even.

By examining E57 Eq. (3.7.17), the square of the $m_i = 0$ Wigner- $3j$ symbol can be expressed as

$$\begin{pmatrix} j_1 & j_2 & j_3 \\ 0 & 0 & 0 \end{pmatrix}^2 = \frac{1}{J+1} \frac{g(p_1)g(p_2)g(p_3)}{g(p)}, \quad (10)$$

where we have introduced the function

$$g(p) = \frac{(2p)!}{2^{2p}(p!)^2}. \quad (11)$$

The factors of 2^{2p} cancel in Eq. (10), but retaining them in Eq. (11) keeps $g(p)$ slowly varying with p , which is advantageous for numerical work. As a guide to its scaling, Stirling's approximation gives $g(p) \sim (\pi p)^{-1/2}$ for large p .

To obtain the recurrence relation used in the algorithm, we rewrite the factorial in Eq. (11) as

$$(2p)! = 2p(2p-1)(2p-2) \cdots 1 = 2^{2p} p! (p - \frac{1}{2})(p - \frac{3}{2}) \cdots \frac{1}{2}.$$

Substituting this into Eq. (11) yields

$$g(p) = \frac{(p - \frac{1}{2})(p - \frac{3}{2}) \cdots \frac{1}{2}}{p!},$$

from which the recurrence

$$g(p) = \frac{p - \frac{1}{2}}{p} g(p-1) \quad (12)$$

follows immediately.

Starting from $g(0) = 1$, Eq. (12) is used to construct $\ln g(p)$ for $p = 1, \dots, p_{\max}$ in linear time, after which both $g(p)$ and its reciprocal $1/g(p)$ are obtained by exponentiation and stored, with $p_{\max} \sim \mathcal{O}(\ell_{\max})$. The factors $(J+1)^{-1}$ required in Eq. (10) are likewise precomputed for the relevant range of J . Once these tables are available, evaluation of the squared $(0, 0, 0)$ symbol reduces to a small number of multiplications and cache-resident array lookups, with no factorials or transcendental functions appearing in the main summation loops.

3.2 Squared Symbol $\mathcal{J}_{(-2,2)}$

The polarization kernels require the symbol

$$\begin{pmatrix} j_1 & j_2 & j_3 \\ -2 & 2 & 0 \end{pmatrix} = \mathcal{J}_{(-2,2)}.$$

To obtain it, we first derive the intermediate expression for the $(0, -2, 2)$ configuration. Applying Eq. (3.7.13) of E57 with $m_1 = 0$,

$m_2 = -1, m_3 = 1$, and shifting $j_3 \mapsto j_3 + 1$, gives

$$\begin{aligned} & \sqrt{(J+2)(J_{-+}+1)(J_{+-}+1)J_{++}} \begin{pmatrix} j_1 & j_2 & j_3+1 \\ 0 & -1 & 1 \end{pmatrix} \\ &= \lambda \begin{pmatrix} j_1 & j_2 & j_3 \\ 0 & 0 & 0 \end{pmatrix} \\ &+ 2\sqrt{j_3(j_3+2)} \begin{pmatrix} j_1 & j_2 & j_3 \\ 0 & -1 & 1 \end{pmatrix} \\ &- \eta \begin{pmatrix} j_1 & j_2 & j_3 \\ 0 & -2 & 2 \end{pmatrix}, \end{aligned} \quad (13)$$

with

$$\begin{aligned} \lambda &= \sqrt{j_2(j_2+1)(j_3+1)(j_3+2)}, \\ \eta &= \sqrt{(j_2-1)(j_2+2)(j_3-1)j_3}. \end{aligned} \quad (14)$$

The two $\mathcal{J}_{(-1,1)}$ symbols in Eq. (13) can be written entirely in terms of $\mathcal{J}_{(0,0)}$ symbols with shifted arguments; these identities are derived in Appendix B. Substituting them into Eq. (13) yields

$$\begin{pmatrix} j_1 & j_2 & j_3 \\ 0 & -2 & 2 \end{pmatrix} = \eta^{-1} \left[\alpha \begin{pmatrix} j_1 & j_2 & j_3 \\ 0 & 0 & 0 \end{pmatrix} + \beta \begin{pmatrix} j_1 & j_2 & j_3+2 \\ 0 & 0 & 0 \end{pmatrix} \right], \quad (15)$$

with α and β given in closed form in Appendix B. Since the coupling matrices involve only the square of this quantity, the algorithm evaluates

$$\begin{pmatrix} j_1 & j_2 & j_3 \\ 0 & -2 & 2 \end{pmatrix}^2 = \eta^{-2} \left(\alpha^2 X^2 + 2\alpha\beta |XY| s(J) + \beta^2 Y^2 \right), \quad (16)$$

where X and Y denote the two $\mathcal{J}_{(0,0)}$ symbols, $|XY| = \sqrt{X^2 Y^2}$, and $s(J)$ is a parity-dependent sign factor. A final even permutation maps the $(0, -2, 2)$ symbol to the required $(-2, 2, 0)$ configuration, as in Eq. (7).

4 SPEED TESTS OF `threej_cosmo`

From this point onward we revert to the standard CMB notation and use ℓ (rather than j) for multipole indices; ℓ_{\max} denotes the maximum multipole used in the coupling-matrix construction. To assess performance, we benchmark the `threej_cosmo` implementation against a reference implementation based on the standard Schulten–Gordon (S-G) recursion, as used in the `pspy` package. The `mcm_compute` module evaluates the mode-coupling matrices using the S-G recursion and is representative of current pseudo- C_ℓ pipelines.

We benchmark using the ACT DR6 survey window map (Naess et al. 2025), which is the same for both temperature and polarization. For each choice of ℓ_{\max} , the mask auto-power spectrum W_ℓ is computed directly from this map using `pixel1` (Naess et al. 2021) by evaluating the spherical-harmonic coefficients of the window up to $2\ell_{\max}$ and forming the auto-spectrum $W_\ell = \frac{1}{2\ell+1} \sum_m |w_{\ell m}|^2$. The factor of $2\ell_{\max}$ reflects the standard pseudo- C_ℓ formalism, which requires W_L for $L \leq 2\ell_{\max}$ in the coupling-matrix construction. Timing tests are performed for ten values of ℓ_{\max} linearly spaced between 500 and 10,000. For each ℓ_{\max} , the resulting W_ℓ is passed identically to both `threej_cosmo` and the S-G-based reference implementation, and the wall-clock runtime of each call is measured. Each test is repeated five times, and we report the mean execution time and standard deviation. All CPU benchmarks are performed on an 8-core Apple M3 processor.

4.1 CPU performance

As seen in Figure 1, the `threej_cosmo` implementation exhibits the expected cubic scaling, $T \propto \ell_{\max}^3$, but with a substantially reduced prefactor compared to the reference S-G recursion. This reduction leads to large and consistent performance gains across the full range of multipoles tested.

For TT coupling matrices, the speedup increases rapidly with ℓ_{\max} , reaching factors of 20–25× for $\ell_{\max} \gtrsim 2000$ and remaining at least 19× faster up to $\ell_{\max} = 10^4$. For example, at $\ell_{\max} = 4722$ the S-G-based runtime is 64.2 s, while `threej_cosmo` completes the same calculation in 2.54 s. At $\ell_{\max} = 10^4$, the TT computation requires ~34 s with `threej_cosmo`, compared with over ten minutes for the S-G implementation.

The EE coupling matrices follow the same overall scaling behaviour but with a smaller relative speedup. At low multipoles the improvement is modest (~1.7× at $\ell_{\max} = 500$), stabilising to 6–7× for $\ell_{\max} \gtrsim 1500$. This difference reflects the additional algebraic operations associated with the $\mathcal{J}_{(-2,2)}$ configuration.

The `threej_cosmo` implementation parallelises the outer loop over ℓ_1 using OpenMP with dynamic scheduling. All intermediate quantities are thread-private, and the coupling matrix is stored in row-major order to ensure contiguous memory access. After computing the upper triangle, the symmetry $K_{\ell_1 \ell_2} = K_{\ell_2 \ell_1}$ is used to fill in the lower triangle. This strategy provides good load balance across the triangular iteration space and avoids redundant computation.

4.2 GPU acceleration

We additionally benchmark a GPU implementation based on OpenMP target offloading, compiled with the NVIDIA HPC SDK and executed on an NVIDIA A100 GPU (40 GB). The GPU kernel reuses the same algorithm as the CPU implementation: each (ℓ_1, ℓ_2) element is computed independently and maps naturally onto fine-grained parallelism.

Figure 2 shows the GPU performance when measuring kernel execution time only, excluding data transfer and kernel-launch overheads. Under this like-for-like comparison, the GPU implementation outperforms the S-G implementation across the entire multipole range tested, including the lowest values of ℓ_{\max} . At $\ell_{\max} = 10^4$, the GPU kernel time is 0.63 s for TT and 3.2 s for EE. This corresponds to speedups of 54× for TT and 35× for EE when compared to the optimized `threej_cosmo` CPU implementation, and exceeds 1000× for TT and 200× for EE when compared directly to the S-G baseline.

The measured GPU kernel times scale as $t \propto \ell_{\max}^3$ for both TT and EE, in close agreement with the theoretical arithmetic complexity of the algorithm.

4.3 Band-limited covariance matrices

As discussed earlier, approximate pseudo- C_ℓ covariance expressions for apodized or otherwise band-limited masks lead to coupling-matrix-like kernels in which the sum over the intermediate multipole ℓ_3 is effectively truncated at a characteristic scale L_{apo} set by the support of the survey window function in harmonic space. In this regime, the incremental algorithm can exploit the reduced coupling width by terminating the internal ℓ_3 summation at a cutoff L_{cut} .

To isolate the performance impact of this effect, we benchmark a modified implementation in which the window-function power spectrum \tilde{W}_{ℓ_3} (defined as the auto-spectrum of the real-space mask) satisfies $\tilde{W}_{\ell_3} = 0$ for $\ell_3 > L_{\text{cut}}$, so that truncating the summation introduces no approximation. This benchmarking is performed on the

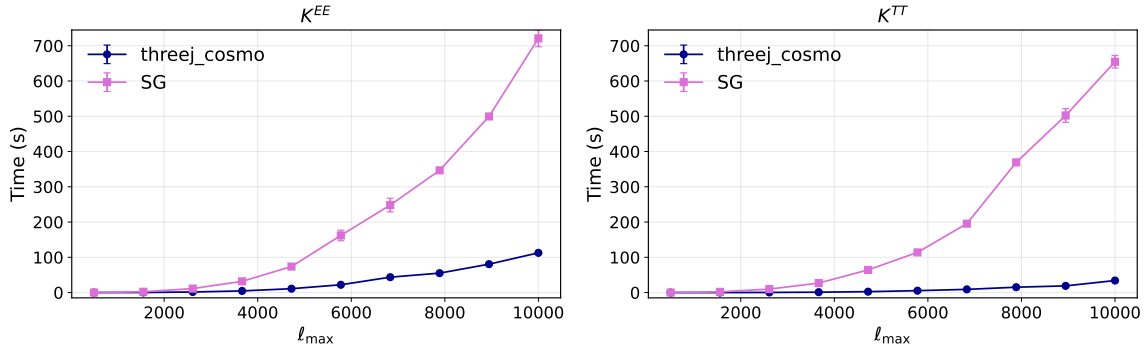


Figure 1. CPU time for the calculation of the mode-coupling matrices K^{EE} (left) and K^{TT} (right) as a function of l_{\max} , comparing the `threej_cosmo` implementation with the reference Schulten–Gordon (S-G) algorithm. Tests use the ACT DR6 mask and were run on an 8-core Apple M3 CPU. Error bars show the standard deviation over 5 runs per l_{\max} . For TT, `threej_cosmo` achieves speedups of $\sim 20\text{--}25\times$ for $l_{\max} \gtrsim 2000$ (e.g. $25.3\times$ at $l_{\max} = 4722$), while for EE the speedup is typically $\sim 6\text{--}7\times$ (e.g. $6.7\times$ at $l_{\max} = 4722$).

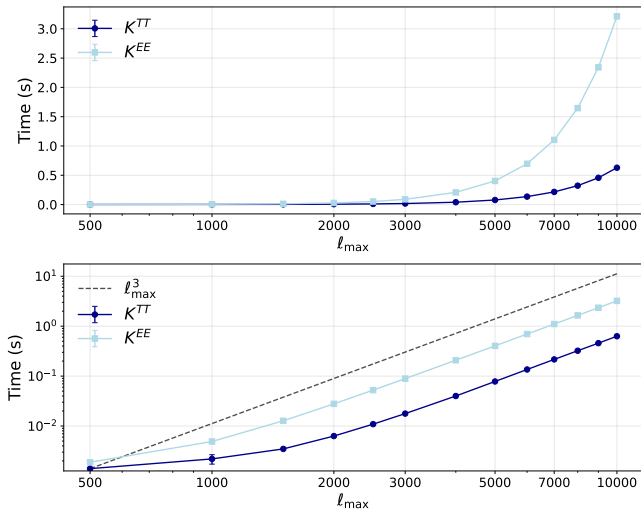


Figure 2. Kernel execution time as a function of multipole moment l_{\max} for the GPU-accelerated `threej_cosmo` code computing K^{TT} and K^{EE} coupling matrices. Benchmarks were performed on an NVIDIA A100 GPU (40 GB) using OpenMP target offloading with linearized triangular iteration for full parallelization. Times shown are kernel execution only, excluding data transfer overhead (~ 0.4 s per invocation). Error bars show the standard deviation over 5 runs. *Top:* Linear scale showing K^{TT} computation completes in 0.63 s and K^{EE} in 3.2 s at $l_{\max} = 10^4$. *Bottom:* Log-log scale with ℓ_{\max}^3 reference line (dashed), confirming the expected cubic scaling.

CPU setup described in Section 4.1. Numerical agreement with both the uncapped `threej_cosmo` implementation and the S-G-based reference is verified at the $10^{-10}\text{--}10^{-14}$ level across all tested multipoles.

In this band-limited setting, speedups relative to the S-G reference become very large, and depend on both l_{\max} and L_{cut} . At fixed L_{cut} , the speedup grows with l_{\max} : for TT coupling at $L_{\text{cut}} = 64$, improvements increase from $\sim 28\times$ at $l_{\max} = 1500$ to $\sim 115\times$ at $l_{\max} = 5000$. At fixed l_{\max} , the speedup decreases as L_{cut} approaches l_{\max} , since the effective summation range widens. For example at $l_{\max} = 3000$, TT speedups range from $\sim 60\times$ at $L_{\text{cut}} = 16$ down to $\sim 21\times$ at $L_{\text{cut}} = 512$. Polarization coupling matrices show comparable or larger gains across the same parameter space, reaching $\sim 480\times$ for EE at $l_{\max} = 5000$ with small L_{cut} . By contrast, the runtime of the S-G implementation is essentially independent of L_{cut} , since it evaluates the full ℓ_3 range for each matrix element.

4.4 Discussion

The benchmarks in Fig. 1 show that the new algorithm delivers substantial and robust speedups over the standard S-G-based Fortran implementation. On the CPU, the runtime follows the expected ℓ_{\max}^3 scaling but with a significantly reduced prefactor, leading to speedups of $20\text{--}25\times$ for TT and $6\text{--}7\times$ for EE at high multipoles. Across all tested configurations, numerical agreement with the Fortran reference is maintained at the level of 10^{-12} .

The GPU results in Fig. 2 illustrate a complementary performance regime. While overheads are significant at low l_{\max} , the GPU becomes increasingly effective for large matrices, ultimately providing an additional order-of-magnitude acceleration relative to the CPU for TT and a factor of several for EE. This behaviour is consistent with the parallel evaluation of independent (j_1, j_2) blocks and the arithmetic intensity of the kernel at high multipoles.

In addition to full matrix construction, the structure of the algorithm is particularly well matched to band-limited coupling calculations. In this case, the incremental formulation allows unnecessary recursion steps to be bypassed, yielding further reductions in computational cost without modifying the core kernel or sacrificing accuracy. This flexibility is relevant for applications involving apodized masks or approximate covariance terms, where coupling support is limited.

5 CONCLUSION

We have presented an efficient method for evaluating the restricted set of Wigner–3 j symbol combinations that arise in CMB pseudo- C_{ℓ} mode-coupling calculations. By expressing both temperature and polarization couplings in terms of a small number of squared $\mathcal{J}_{(0,0)}$ symbols, and obtaining more complex configurations algebraically from these base quantities, the method avoids redundant calculations.

The resulting implementation retains the formal $\mathcal{O}(\ell_{\max}^3)$ scaling of standard approaches but with a reduced computational cost, while maintaining numerical accuracy at the level required for precision CMB analyses. The same kernel is readily parallelised on both CPUs and GPUs, enabling efficient execution across a range of architectures.

The formulation is suited to scenarios in which only a restricted set of coupling modes is required, such as band-limited coupling matrices and analytic covariance constructions. As a result, `threej_cosmo` provides a lightweight, accurate, and scalable backend for pseudo-

C_ℓ pipelines, with direct relevance for current and upcoming CMB experiments.

Our approach could be extended beyond the $\mathcal{J}_{(0,0)}$, $\mathcal{J}_{(-1,1)}$ and $\mathcal{J}_{(-2,2)}$ symbols. For example in the analysis of the stochastic gravitational wave background (see e.g. Inomata et al. (2024)) the symbols with magnetic numbers $(1, 1, -2)$ and $(2, 2, -4)$ also appear. It would be interesting to see if similar speed-ups are achievable for these symbols also.

Planck Collaboration 2014a, *Astronomy & Astrophysics*, 571, A17
 Planck Collaboration 2014b, *Astron. Astrophys.*, 571, A27
 Planck Collaboration 2020, *Astron. Astrophys.*, 641, A6
 Schulten K., Gordon R. G., 1975, *J. Math. Phys.*, 16, 1961
 Simons Observatory Collaboration 2019, *JCAP*, 2019, 056
 Smoot G. F., et al., 1992, *Astrophys. J.*, 396, L1
 Wandelt B. D., Hivon E., Górski K. M., 2001, *Phys. Rev. D*, 64, 083003

ACKNOWLEDGEMENTS

We thank Anthony Challinor and George Efstathiou for useful discussions and Roger de Belsunce for helpful comments on a draft of this paper. This work was performed using resources provided by the Cambridge Service for Data Driven Discovery (CSD3) operated by the University of Cambridge Research Computing Service (www.csd3.cam.ac.uk), provided by Dell EMC and Intel using Tier-2 funding from the Engineering and Physical Sciences Research Council (capital grant EP/T022159/1), and DiRAC funding from the Science and Technology Facilities Council (www.dirac.ac.uk) funded by BEIS capital funding via STFC Capital Grants ST/P002307/1 and ST/R002452/1 and STFC Operations Grant ST/R00689X/1. The authors acknowledge funding from EPSRC ExCALIBUR H&SE grant EP/Y028082/1 and STFC Astronomy Consolidated Grant ST/X001113/1. G.K. is supported by the STFC CDT (Data Intensive Science) grant ST/W006812/1.

DATA AVAILABILITY

The code developed for this work, `threej_cosmo`, is publicly available at https://github.com/gkiddier22/threej_cosmo. No new observational data were generated or analysed in this study.

REFERENCES

Alonso D., Sanchez J., Slosar A., 2019, *Mon. Not. R. Astron. Soc.*, 484, 4127
 Brown M. L., Castro P. G., Taylor A. N., 2005, *Mon. Not. R. Astron. Soc.*, 360, 1262
 Edmonds A. R., 1957, Angular Momentum in Quantum Mechanics. Princeton University Press, Princeton, NJ
 Efstathiou G., 2004, *Mon. Not. R. Astron. Soc.*, 349, 603
 Harscouet L., Cowell J. A., Ereza J., Alonso D., Camacho H., Nicola A., Slosar A., 2025, *The Open Journal of Astrophysics*, 8
 Hinshaw G., et al., 2013, *The Astrophysical Journal Supplement Series*, 208, 19
 Hivon E., Górski K. M., Netterfield C. B., Crill B. P., Prunet S., Hansen F., 2002, *Astrophys. J.*, 567, 2
 Inomata K., Kamionkowski M., Toral C. M., Taylor S. R., 2024, *Phys. Rev. D*, 110, 063547
 Lizancos A. B., White M., 2024, Harmonic analysis of discrete tracers of large-scale structure, doi:10.48550/arXiv.2312.12285, <http://arxiv.org/abs/2312.12285>
 Louis T., Naess S., Garrido X., Challinor A., 2020, *Physical Review D*, 102, 123538
 Naess S., Madhavacheril M., Hasselfield M., 2021, Pixell: Rectangular pixel map manipulation and harmonic analysis library, Astrophysics Source Code Library, record ascl:2102.003 (ascl:2102.003), <https://ascl.net/2102.003>
 Naess S., et al., 2025, The Atacama Cosmology Telescope: DR6 Maps (arXiv:2503.14451), <https://arxiv.org/abs/2503.14451>
 Okamoto T., Hu W., 2003, *Physical Review D*, 67, 083002
 Penzias A. A., Wilson R. W., 1965, *Astrophys. J.*, 142, 419

APPENDIX A: COUPLING MATRICES

The pseudo- C_ℓ formalism expresses the mode coupling induced by a survey window function through a set of geometry-dependent kernels Ξ_{XY} , where $X, Y \in \{T, E, B\}$. Each coupling matrix can be written in the generic form

$$K_{\ell_1 \ell_2}^{X_i Y_j} = (2\ell_2 + 1) \Xi_{XY}(\ell_1, \ell_2, \tilde{W}^{X_i Y_j}),$$

where $\tilde{W}_\ell^{X_i Y_j}$ denotes the harmonic power spectrum of the survey window function for the map pair (X_i, Y_j) . The explicit form of Ξ_{XY} is determined by combinations of Wigner- $3j$ symbols and is given below for each case.

All expressions in this section use the shorthand

$$L \equiv \ell_1 + \ell_2 + \ell_3,$$

where ℓ_3 denotes the intermediate multipole summed over in the coupling-matrix construction.

Temperature–temperature (TT). Only the symbol with $m_i = 0$ appears:

$$\Xi_{TT}(\ell_1, \ell_2, \tilde{W}) = \frac{1}{4\pi} \sum_{\ell_3} (2\ell_3 + 1) \tilde{W}_{\ell_3} \begin{pmatrix} \ell_1 & \ell_2 & \ell_3 \\ 0 & 0 & 0 \end{pmatrix}^2. \quad (\text{A1})$$

Temperature–polarization (TE). The TE coupling involves the product of the $m_i = 0$ and $m_1 = -2, m_2 = 2, m_3 = 0$ Wigner- $3j$ symbols and is non-zero only for even L :

$$\Xi_{TE}(\ell_1, \ell_2, \tilde{W}) = \frac{1}{4\pi} \sum_{\ell_3} (2\ell_3 + 1) \tilde{W}_{\ell_3} \frac{1 + (-1)^L}{2} \begin{pmatrix} \ell_1 & \ell_2 & \ell_3 \\ 0 & 0 & 0 \end{pmatrix} \begin{pmatrix} \ell_1 & \ell_2 & \ell_3 \\ -2 & 2 & 0 \end{pmatrix}. \quad (\text{A2})$$

E–E polarization (EE). This case involves only the $m_1 = -2, m_2 = 2, m_3 = 0$ symbols and is likewise restricted to even L :

$$\Xi_{EE}(\ell_1, \ell_2, \tilde{W}) = \frac{1}{4\pi} \sum_{\ell_3} (2\ell_3 + 1) \tilde{W}_{\ell_3} \left[\frac{1 + (-1)^L}{2} \right]^2 \begin{pmatrix} \ell_1 & \ell_2 & \ell_3 \\ -2 & 2 & 0 \end{pmatrix}^2. \quad (\text{A3})$$

E–B and B–E (EB/BE). These couplings vanish for even L and are non-zero only for odd parity:

$$\Xi_{EB}(\ell_1, \ell_2, \tilde{W}) = \frac{1}{4\pi} \sum_{\ell_3} (2\ell_3 + 1) \tilde{W}_{\ell_3} \left[\frac{1 - (-1)^L}{2} \right]^2 \begin{pmatrix} \ell_1 & \ell_2 & \ell_3 \\ -2 & 2 & 0 \end{pmatrix}^2. \quad (\text{A4})$$

The same expression holds for Ξ_{BE} .

B–B polarization (BB). The BB coupling kernel has the same structure and parity selection as the EE case, differing only in the underlying power spectrum entering the pseudo- C_ℓ relation.

APPENDIX B: $3j$ SYMBOLS

B1 Obtaining $\mathcal{J}_{(-1,1)}$ symbols

Using Eqs. (3.7.13) and (3.7.15) of E57, and Eq. (9), gives for odd J :

$$\begin{pmatrix} j_1 & j_2 & j_3 \\ 0 & -1 & 1 \end{pmatrix} = -\frac{1}{2} \left[\frac{(J+2)(J_{-++}+1)(J_{+-+}+1)(J_{++-})}{j_2(j_2+1)j_3(j_3+1)} \right]^{1/2} \times \begin{pmatrix} j_1 & j_2 & j_3+1 \\ 0 & 0 & 0 \end{pmatrix}. \quad (\text{B1})$$

For even J , we apply Eq. (3.7.12) of E57 twice. First, for $(m_1, m_2, m_3) = (0, -\frac{1}{2}, \frac{1}{2})$ with $j_2 \mapsto j_2 + \frac{1}{2}$ and $j_3 \mapsto j_3 + \frac{1}{2}$:

$$\sqrt{(J+2)(J_{-++}+1)} \begin{pmatrix} j_1 & j_2 + \frac{1}{2} & j_3 + \frac{1}{2} \\ 0 & -\frac{1}{2} & \frac{1}{2} \end{pmatrix} = \sqrt{j_2 j_3} \begin{pmatrix} j_1 & j_2 & j_3 \\ 0 & -1 & 1 \end{pmatrix} - \sqrt{(j_2+1)(j_3+1)} \begin{pmatrix} j_1 & j_2 & j_3 \\ 0 & 0 & 0 \end{pmatrix}. \quad (\text{B2})$$

Applying Eq. (3.7.12) of E57 again with $m = 0$ and shifting $j_2 \mapsto j_2 + 1, j_3 \mapsto j_3 + 1$:

$$\begin{pmatrix} j_1 & j_2 + \frac{1}{2} & j_3 + \frac{1}{2} \\ 0 & -\frac{1}{2} & \frac{1}{2} \end{pmatrix} = \frac{1}{2} \left[\frac{(J+3)(J_{-++}+2)}{(j_2+1)(j_3+1)} \right]^{1/2} \begin{pmatrix} j_1 & j_2 + 1 & j_3 + 1 \\ 0 & 0 & 0 \end{pmatrix}. \quad (\text{B3})$$

Substituting Eq. (B3) into Eq. (B2), we obtain

$$\begin{pmatrix} j_1 & j_2 & j_3 \\ 0 & -1 & 1 \end{pmatrix} = \left[\frac{(j_2+1)(j_3+1)}{j_2 j_3} \right]^{1/2} \begin{pmatrix} j_1 & j_2 & j_3 \\ 0 & 0 & 0 \end{pmatrix} + \frac{1}{2} \left[\frac{(J+2)(J+3)(J_{-++}+1)(J_{++-}+2)}{j_2(j_2+1)j_3(j_3+1)} \right]^{1/2} \times \begin{pmatrix} j_1 & j_2 + 1 & j_3 + 1 \\ 0 & 0 & 0 \end{pmatrix}. \quad (\text{B4})$$

B2 Further Expressions for $\mathcal{J}_{(-1,1)}$ symbols

From Eq. (13), we need $m_1 = 0, m_2 = -1, m_3 = 1$ symbols for both (j_1, j_2, j_3) and $(j_1, j_2, j_3 + 1)$. For odd J , Eq. (B1) provides $\begin{pmatrix} j_1 & j_2 & j_3 \\ 0 & -1 & 1 \end{pmatrix}$, while for $\begin{pmatrix} j_1 & j_2 & j_3 + 1 \\ 0 & -1 & 1 \end{pmatrix}$, we shift $j_3 \mapsto j_3 + 1$ in Eq. (B4):

$$\begin{pmatrix} j_1 & j_2 & j_3 + 1 \\ 0 & -1 & 1 \end{pmatrix} = \left[\frac{(j_2 + 1)(j_3 + 2)}{j_2(j_3 + 1)} \right]^{1/2} \begin{pmatrix} j_1 & j_2 & j_3 + 1 \\ 0 & 0 & 0 \end{pmatrix} + \frac{1}{2} \left[\frac{(J + 3)(J + 4)(J_{-++} + 2)(J_{-++} + 3)}{j_2(j_2 + 1)(j_3 + 1)(j_3 + 2)} \right]^{1/2} \times \begin{pmatrix} j_1 & j_2 + 1 & j_3 + 2 \\ 0 & 0 & 0 \end{pmatrix}. \quad (\text{B5})$$

If J is even, we can directly use Eq. (B4) to obtain $\begin{pmatrix} j_1 & j_2 & j_3 \\ 0 & -1 & 1 \end{pmatrix}$. However, for $\begin{pmatrix} j_1 & j_2 & j_3 + 1 \\ 0 & -1 & 1 \end{pmatrix}$, we must use Eq. (B1), shifting j_3 to $j_3 + 1$:

$$\begin{pmatrix} j_1 & j_2 & j_3 + 1 \\ 0 & -1 & 1 \end{pmatrix} = -\frac{1}{2} \left[\frac{(J + 3)(J_{-++} + 2)(J_{-++} + 2)(J_{++-} - 1)}{j_2(j_2 + 1)(j_3 + 1)(j_3 + 2)} \right]^{1/2} \times \begin{pmatrix} j_1 & j_2 & j_3 + 2 \\ 0 & 0 & 0 \end{pmatrix}. \quad (\text{B6})$$

B3 Closed-form reduction of $\mathcal{J}_{(-2,2)}$

We derive the two-term closed form for the $\mathcal{J}_{(-2,2)}$ configuration used in the implementation. We define

$$\begin{aligned} \lambda &\equiv \sqrt{j_2(j_2 + 1)(j_3 + 1)(j_3 + 2)}, \\ \eta &\equiv \sqrt{(j_2 - 1)(j_2 + 2)(j_3 - 1)j_3}, \end{aligned} \quad (\text{B7})$$

and use the standard triangle combinations as in Eq. (8).

Starting from Eq. (13), we rewrite it as

$$\eta \begin{pmatrix} j_1 & j_2 & j_3 \\ 0 & -2 & 2 \end{pmatrix} = \lambda \begin{pmatrix} j_1 & j_2 & j_3 \\ 0 & 0 & 0 \end{pmatrix} + 2\sqrt{j_3(j_3 + 2)} \begin{pmatrix} j_1 & j_2 & j_3 \\ 0 & -1 & 1 \end{pmatrix} - \Lambda \begin{pmatrix} j_1 & j_2 & j_3 + 1 \\ 0 & -1 & 1 \end{pmatrix}, \quad (\text{B8})$$

where

$$\Lambda \equiv \sqrt{(J + 2)(J_{-++} + 1)(J_{-++} + 1)J_{++-}}. \quad (\text{B9})$$

For even J , the symbol $\begin{pmatrix} j_1 & j_2 & j_3 \\ 0 & -1 & 1 \end{pmatrix}$ reduces to a single $(0, 0, 0)$ symbol,

$$\begin{pmatrix} j_1 & j_2 & j_3 \\ 0 & -1 & 1 \end{pmatrix} = \sqrt{\frac{(j_2 + 1)(j_3 + 1)}{j_2 j_3}} \left(1 - \frac{(J + 2)(J_{-++} + 1)}{2(j_2 + 1)(j_3 + 1)} \right) \times \begin{pmatrix} j_1 & j_2 & j_3 \\ 0 & 0 & 0 \end{pmatrix}, \quad (\text{B10})$$

while the shifted symbol $\begin{pmatrix} j_1 & j_2 & j_3 + 1 \\ 0 & -1 & 1 \end{pmatrix}$ has odd total angular momentum and is therefore given by

$$\begin{pmatrix} j_1 & j_2 & j_3 + 1 \\ 0 & -1 & 1 \end{pmatrix} = -\frac{1}{2} \left[\frac{(J + 3)(J_{-++} + 2)(J_{-++} + 2)(J_{++-} - 1)}{j_2(j_2 + 1)(j_3 + 1)(j_3 + 2)} \right]^{1/2} \times \begin{pmatrix} j_1 & j_2 & j_3 + 2 \\ 0 & 0 & 0 \end{pmatrix}. \quad (\text{B11})$$

Substituting Eq. (B10) into the second term of Eq. (B8) gives

$$2\sqrt{j_3(j_3 + 2)} \begin{pmatrix} j_1 & j_2 & j_3 \\ 0 & -1 & 1 \end{pmatrix} = \frac{2\lambda}{j_2} \left(1 - \frac{(J + 2)(J_{-++} + 1)}{2(j_2 + 1)(j_3 + 1)} \right) \begin{pmatrix} j_1 & j_2 & j_3 \\ 0 & 0 & 0 \end{pmatrix}, \quad (\text{B12})$$

where we used $\lambda^2 = j_2(j_2 + 1)(j_3 + 1)(j_3 + 2)$.

Similarly, substituting Eq. (B11) into the third term of Eq. (B8) yields

$$-\Lambda \begin{pmatrix} j_1 & j_2 & j_3 + 1 \\ 0 & -1 & 1 \end{pmatrix} = \frac{1}{2\lambda} [(J + 2)(J_{-++} + 1)(J_{-++} + 1)J_{++-} \times (J + 3)(J_{-++} + 2)(J_{-++} + 2)(J_{++-} - 1)]^{1/2} \times \begin{pmatrix} j_1 & j_2 & j_3 + 2 \\ 0 & 0 & 0 \end{pmatrix}. \quad (\text{B13})$$

Collecting terms and dividing by η , we obtain the final two-term reduction

$$\begin{pmatrix} j_1 & j_2 & j_3 \\ 0 & -2 & 2 \end{pmatrix} = \eta^{-1} \left[\alpha \begin{pmatrix} j_1 & j_2 & j_3 \\ 0 & 0 & 0 \end{pmatrix} + \beta \begin{pmatrix} j_1 & j_2 & j_3 + 2 \\ 0 & 0 & 0 \end{pmatrix} \right], \quad (\text{B14})$$

with coefficients

$$\alpha = \lambda + \frac{2\lambda}{j_2} \left(1 - \frac{(J + 2)(J_{-++} + 1)}{2(j_2 + 1)(j_3 + 1)} \right), \quad (\text{B15})$$

$$\beta = \frac{1}{2\lambda} [(J + 2)(J_{-++} + 1)(J_{-++} + 1)J_{++-} \times (J + 3)(J_{-++} + 2)(J_{-++} + 2)(J_{++-} - 1)]^{1/2}. \quad (\text{B16})$$

Equation (B14) is used in the `threej_cosmo` implementation: the $\mathcal{J}_{(-2,2)}$ symbol is evaluated using two $\mathcal{J}_{(0,0)}$ symbols at (j_1, j_2, j_3) and $(j_1, j_2, j_3 + 2)$, together with the standard parity phase relating the two $(0, 0, 0)$ symbols.

B4 Possible simplification for even J for $\mathcal{J}_{(-1,1)}$ symbols

As written, Eq. (B4) requires the evaluation of two $\mathcal{J}_{(0,0)}$ symbols. However, we can use Eqs. (10) and (12) to write the square of one in terms of the square of the other (and then use Eq. (3.7.17) of E57 to restore the sign). We find

$$\begin{pmatrix} j_1 & j_2 + 1 & j_3 + 1 \\ 0 & 0 & 0 \end{pmatrix} = - \left[\frac{(J+2)(J_{-++} + 1)}{(J+3)(J_{-++} + 2)} \right]^{1/2} \times \begin{pmatrix} j_1 & j_2 & j_3 \\ 0 & 0 & 0 \end{pmatrix}. \quad (\text{B17})$$

Using this, Eq. (B4) gives

$$\begin{pmatrix} j_1 & j_2 & j_3 \\ 0 & -1 & 1 \end{pmatrix} = \left[\frac{(j_2 + 1)(j_3 + 1)}{j_2 j_3} \right]^{1/2} \left(1 - \frac{(J+2)(J_{-++} + 1)}{2(j_2 + 1)(j_3 + 1)} \right) \times \begin{pmatrix} j_1 & j_2 & j_3 \\ 0 & 0 & 0 \end{pmatrix}. \quad (\text{B18})$$